

May 2019

## Equation of State of H<sub>2</sub>O Ice Using Melt-Recrystallization

Zachary Michael Grande  
zachgrande@gmail.com

Follow this and additional works at: <https://digitalscholarship.unlv.edu/thesesdissertations>



Part of the [Condensed Matter Physics Commons](#), [Engineering Science and Materials Commons](#), and the [Materials Science and Engineering Commons](#)

---

### Repository Citation

Grande, Zachary Michael, "Equation of State of H<sub>2</sub>O Ice Using Melt-Recrystallization" (2019). *UNLV Theses, Dissertations, Professional Papers, and Capstones*. 3605.  
<https://digitalscholarship.unlv.edu/thesesdissertations/3605>

This Thesis is protected by copyright and/or related rights. It has been brought to you by Digital Scholarship@UNLV with permission from the rights-holder(s). You are free to use this Thesis in any way that is permitted by the copyright and related rights legislation that applies to your use. For other uses you need to obtain permission from the rights-holder(s) directly, unless additional rights are indicated by a Creative Commons license in the record and/or on the work itself.

This Thesis has been accepted for inclusion in UNLV Theses, Dissertations, Professional Papers, and Capstones by an authorized administrator of Digital Scholarship@UNLV. For more information, please contact [digitalscholarship@unlv.edu](mailto:digitalscholarship@unlv.edu).

EQUATION OF STATE OF H<sub>2</sub>O ICE USING MELT-RECRYSTALLIZATION

By

Zachary M. Grande

Bachelor of Science – Physics  
University of Nevada, Las Vegas  
2015

A thesis submitted in partial fulfillment  
of the requirements for the

Master of Science – Physics

Department of Physics and Astronomy  
College of Sciences  
The Graduate College

University of Nevada, Las Vegas  
May 2019

Copyright [2019] by [Zachary Grande] All Rights Reserved



## Thesis Approval

The Graduate College  
The University of Nevada, Las Vegas

April 9, 2019

This thesis prepared by

Zachary M. Grande

entitled

Equation of State of H<sub>2</sub>O Ice Using Melt-Recrystallization

is approved in partial fulfillment of the requirements for the degree of

Master of Science – Physics  
Department of Physics and Astronomy

Ashkan Salamat, Ph.D.  
*Examination Committee Chair*

Kathryn Hausbeck Korgan, Ph.D.  
*Graduate College Dean*

Jason Steffen, Ph.D.  
*Examination Committee Member*

Stephen Lepp, Ph.D.  
*Examination Committee Member*

Oliver Tschauner, Ph.D.  
*Examination Committee Member*

Paul Forster, Ph.D.  
*Graduate College Faculty Representative*

**Abstract:**

The recent surge in exoplanet discoveries due to advancements in astrophysical technology and analysis has brought the reliability of early equation of state measurements into question as they are the limiting factor when modeling composition of these planets. H<sub>2</sub>O content is among the most important for the search of habitable planets as well as in understanding planetary dynamics and atmosphere formation. Over the last three decades the equation of state of H<sub>2</sub>O has been investigated with various techniques but, has suffered from anisotropic strain and poor powder statistics resulting in a large discrepancy in equation of state fits. At pressures within the interior of many planets, the hydrogen bonds in H<sub>2</sub>O gradually weaken and are replaced by ionic bonds in ice-X. By melt-recrystallization of ice *via* laser heating as it is compressed, we observe the transition from ice-VII to ice X at a pressure of  $30.9 \pm 2.9$  GPa, evidenced by an abrupt 2.5-fold increase in bulk modulus, implying an increase in bond strength. This transition is preceded by a modified ice structure of tetragonal symmetry, ice-VII<sub>t</sub>.

## **Acknowledgements:**

This research was sponsored in part by the National Nuclear Security Administration under the Stewardship Science Academic Alliances program through DOE Cooperative Agreement \#DE-NA0001982.

This work was performed at HPCAT (Sector 16), Advanced Photon Source (APS), Argonne National Laboratory.

HPCAT operation is supported by DOE-NNSA under Award No. DE-NA0001974, with partial instrumentation funding by NSF.

The project was conceived through collaboration between Ashkan Salamat, Oliver Tschauner, and Jason Steffen.

Beam line support was provided by Jesse Smith of HPCAT.

Analysis was aided by Jonh H. Boisvert.

Laser Heating experiments were aided by Dean Smith and Christian Childs.

**Dedication:**

I would like to dedicate this work to my companion and friend, Hercules, for moral support throughout my project.

**Table of Contents:**

**Abstract:** ..... **iii**

**Acknowledgements:** ..... **iv**

**Dedication:** ..... **v**

**List of Figures:** ..... **viii**

**List of Equations:** ..... **ix**

**Introduction:**..... **1**

**High Pressure H<sub>2</sub>O ices:**..... **3**

**LH-DAC:**..... **6**

**Equation of State of Ice:**..... **8**

**X-ray Diffraction:**..... **12**

**Methods:**..... **15**

**Results:**..... **21**

**Conclusion:** ..... **27**

**Bibliography:** ..... **29**



**Curriculum Vitae: ..... 32**

**List of Figures:**

**Figure 1: SEM image of indented Re gasket using 50  $\mu\text{m}$  culet diamonds with sample chamber formed by focus ion beam micro-machining..... 7**

**Figure 2: Comparison of XRD 2-D images on *Pilatus* detector for ice-VII..... 17**

**Figure 3: Platinum lined gasket. ... 18**

**Figure 4: Preparation of powdered ice-VII. .... 20**

**Figure 5: Demonstration of failure to fit data to a single phase. .... 22**

**Figure 6: Evidence for transition to tetragonal ice-VII<sub>t</sub>. .... 23**

**Figure 7: Successful fit using 3 phase model. .... 26**

**Figure 8: High-pressure high-temperature phase diagram of H<sub>2</sub>O.. .... 28**

**List of Equations:**

<b>Equation 1</b> .....	<b>8</b>
<b>Equation 2</b> .....	<b>8</b>
<b>Equation 3</b> .....	<b>9</b>
<b>Equation 4</b> .....	<b>9</b>
<b>Equation 5</b> .....	<b>9</b>
<b>Equation 6</b> .....	<b>10</b>
<b>Equation 7</b> .....	<b>10</b>
<b>Equation 8</b> .....	<b>12</b>
<b>Equation 9</b> .....	<b>12</b>
<b>Equation 10</b> .....	<b>13</b>
<b>Equation 11</b> .....	<b>13</b>
<b>Equation 12:</b> .....	<b>21</b>

**Introduction:**

H<sub>2</sub>O is the most abundant compound in the solar system and, most likely, the universe. Because of this wide-spread abundance, it plays a vital role in determining planetary properties from: internal dynamics and differentiation, atmosphere formation, plate tectonics in geologically active bodies, and defining habitability of planets. In order to pin point the mechanisms with which H<sub>2</sub>O controls these properties, a better understanding of how it behaves at the conditions found within planetary bodies is needed.

This simple molecule turns out to have one of the most complicated thermodynamic phase diagrams, creating complications when trying to understand its exact role in governing the properties of planets. Within the conditions experienced in our everyday life on the surface of Earth, we regularly observe three of these phases: ice-I<sub>h</sub>, liquid water, and water vapor (and clathrates at the bottom of the ocean). Percy Bridgman realized in the early 20<sup>th</sup> century that these three phases were only the surface of a much more complex phase diagram, as he discovered four additional solid phases at low temperature and pressures below 1 GPa (*Bridgman, 1912*). Static measurements have now been conducted from 2000 K down to millikelvin temperatures and pressures of up to 210 GPa, revealing: at least 17 solid crystalline phases of H<sub>2</sub>O ice, several amorphous phases, and the fluid states (*Duneva et al. 2010, Goncharov et al. 1996*). While dynamic compression experiments have reached over 300 GPa and near 9000K which have led to observations of several possible conductive states (*Millot et al. 2018*). However, nearly all states besides liquid, vapor and ice-I<sub>h</sub> are metastable at conditions that can only be obtained in a cryogenic

laboratory experiments or deep within a planet; replicating the latter is the focus of my Master's work.

Venturing deep within a planet to discover its structure is an idea first coined by Jules Verne's classic *Journey to the Center of the Earth*. As in many cases, this science fiction paved the way for scientific discovery in the pursuit of understanding the effect on materials subjugated to the extreme temperatures and enormous pressures deep within a planet caused by the crushing gravitational force of the planetary mass above. This lays out the thermodynamic conditions that must be replicated in the lab to aid in characterizing the properties of H<sub>2</sub>O within a planet.

### **High Pressure H<sub>2</sub>O ices:**

The complex polymorphism in H<sub>2</sub>O ices arises from the weak nature of the hydrogen bond (H-bond) which is characteristic of all ice structures besides ice-X. These H-bonds are established through correlated disorder between the protons and adjacent oxygens so that, at each moment two hydrogens and one oxygen form an H<sub>2</sub>O molecule. At low to moderate pressures, the complexity in ice structures arise from the steric rearrangement of the H-bonds between molecules while in each independent molecule, the H-O-H bond angle and distance remains mostly constant. The H-bonds in H<sub>2</sub>O ices exhibit a network like structure similar to silica and silicates.

At room temperature and pressures above 2.7 GPa ice-VII becomes the dominant structure for H<sub>2</sub>O ice (*Bridgman, 1937, Bezacier et al. 2014*). This consists of a body centered cubic oxygen structure whose symmetry is lowered into a primitive cell (*Pn-3m*) due to the H-bonded network and is commonly acknowledged as the H-disordered analogue to ordered, tetragonal, ice-VIII. H-ordered and disordered ices refer to their adherence to the Bernal-Fowler 'ice rules' (*Dunaeva et al. 2010*). These are the classical rules used to characterize an ice which state: 1. each oxygen is covalently bonded to two hydrogens and 2. each oxygen forms two hydrogen bonds with adjacent oxygens. However, all ices including ice-VII create a grey area because generally they adhere to these rules but, exhibits microscopic H-disorder. This arises because of the high symmetry structure of the O-H---O bond causing the hydrogens to experience a double well potential between the two oxygens, stimulating quantum mechanical tunneling between the two sites so that, they occupy two different Wyckoff positions in the lattice, with half occupancy. Effectively this

means, that at each moment the ice rules are not broken in but, the time averaged structure exhibits an H-disordered structure.

When compressed to the high pressures found within the Earth, Neptune, and water-rich super earths the already weakened H-bonds in ice-VII continue to weaken as the two potential wells begin to increasingly overlap causing the barrier between them to become increasingly shallower. This continues until finally, they collapse into a single well directly in the center of the two oxygen atoms breaking the H-bond network, which is replaced by an ionic O-H-O bond in, symmetric, ice-X (*Holzappel, 1972*). The point at which this transition occurs in room temperature high pressure ice-VII is a topic of much debate within the water community.

Claims for the transition from ice-VII to X have been made as low as 40 GPa through X-ray diffraction (XRD) data based on the equation of state and comparison between the 111 peak (which is solely contributed to by the hydrogen position) and the 222 peak (*Loubeyre et al. 1999*). However, XRD scattering cross section goes as  $Z^2$  (where Z is the atomic charge/ number of electrons of each atom) so that the ionized hydrogen (proton) is nearly invisible to this probe. Because of this, studies which are sensitive to the protons position were investigated. Raman spectroscopy by *Goncharov et al. 1999* was thought to confirm the transition near 60 GPa as they observed the disappearance of all vibrational modes and the emergence of the  $T_{1g}$  mode which is characteristic of the cuprit-like structure in ice-X. In the Raman study by *Zha et al. 2016* a more sophisticated approach was taken to correct for the diamond background and they report observation of the ice-VII structure beyond 120 GPa. Most recently, *Meier et al. 2018* reported H-NMR data where the

transition from a double well to a single well was reported to take place sluggishly from 75 to 90 GPa. These discrepancies illustrate the problem that the ice-VII structure is continuously changing with density due to an increased symmetry of attraction by the hydrogen to each oxygen atom. The question remains whether the symmetrization process is an abrupt collapse of the double well potential or a sluggish transition that occurs over a wide range of pressures.

Further peculiarities have arisen from taking into consideration these intermediate steps from ice-VII to ice-X. This begins with the 'modulated ice phases' coined in *Loubeyre et al. 1999* original paper claiming ice-X. Through neutron diffraction, which is particularly sensitive to the proton position, *Guthrie et al. 2013* find improved fitting to their data with a model which accommodates interstitial site occupancy of the protons beginning near 13 GPa which began the idea of a further disordered ice-VII' phase.



**LH-DAC:**

As a condensed matter physicist focusing on high pressures and temperatures, the laser heated diamond anvil cell (LH-DAC) is the crown jewel of static high pressure and temperature research. DACs are designed to utilize the optical transparency and superior strength of diamonds with very finely polished, flattened tips (culets). This allows high pressure scientists to reach extreme pressures with the modest load of turning a screw. Culet sizes range on the order of 10's to 100's  $\mu\text{m}$  depending on the pressure range of interest in the experiment (smaller culets for higher pressures). Two opposing diamonds are aligned and used to indent a gasket before a sample chamber is machined in the center (Fig. 1). Gaskets are used to constrict the sample between the two opposing diamonds which increases the hydrostaticity of the uniaxial compression supplied by the opposing diamonds. For this, a malleable material is needed that can easily flow with compression of the sample and a high tensile strength is needed to withstand the large uniaxial load being applied by the diamonds. For all experiments in the project being presented here, rhenium foil was used with a starting thickness of 250  $\mu\text{m}$  and final gasket thickness between 10 to 30  $\mu\text{m}$ .

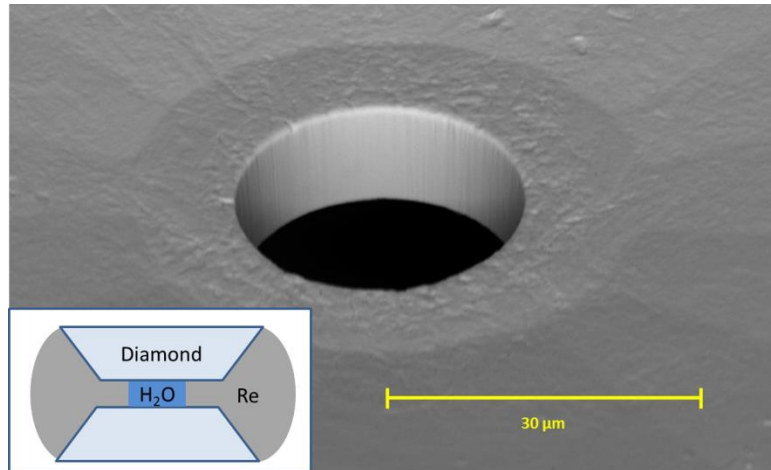


**Figure 1: SEM image of indented Re gasket using 50  $\mu\text{m}$  culet diamonds with sample chamber formed by focus ion beam micro-machining. (Insert: schematic of DAC showing opposing diamonds with Re gasket loaded with  $\text{H}_2\text{O}$  in the sample chamber.)**

In order to achieve high pressures as well as high temperatures we couple the DAC with different laser heating methods which vary with the material being studied. For metallic materials with a large density of free electrons in an ‘electron gas’ like structure, a near-infrared (IR) laser which emits at about  $1 \mu\text{m}$  is used to couple with the metal. This is done by direct absorption of the IR photons by the electrons of the metal, thereby increasing their kinetic energy and consequently raising the temperature of the material by transmitting this heat energy as phonons. In electrically insulating materials, like  $\text{H}_2\text{O}$ , mid-IR ( $10 \mu\text{m}$ ) laser heating is used which is absorbed directly by the intramolecular bonds of the material increasing the kinetic energy of the atoms in the molecule. This kinetic energy promotes transitions in vibrational and rotational states in the solid which is again transmitted as heat by phonons raising the temperature of the bulk material. For  $\text{H}_2\text{O}$ , the absorption of  $10 \mu\text{m}$  radiation occurs through increased population of higher energy vibrational states in the O-H bonds (*Holzappel et al. 1984*).

### Equation of State of Ice:

The most fundamental measurement for planetary modelling is the equation of state (EoS) of the constituent materials in the planet. Simply put, this is a relationship of the thermodynamic variables (pressure (P)-volume (V)-temperature (T)) for solids, analogous to the ideal gas law for gases. For experimental practicality in static compression, the isothermal (T = constant) EoS is normally measured and then thermal expansion is measured separately to give a full EoS. The equations governing the isothermal EoS of solids are derived in terms of the empirically measured parameter the compressibility, or more commonly its inverse (incompressibility) of a material with respect to its 'zero pressure volume' known as the bulk modulus ( $B_0$ ) and its pressure derivate(s):

**Equation 1**  $B_0 = -V_0 \left. \frac{dP}{dV} \right|_{P=0}$

Generally there are two functions that are used in the field of high pressure science, which are derived through different assumptions and goals but, both only assume hydrostatic compression and a data set describing a single phase. The first and probably most well-known and widely used is the Birch-Murnaghan EoS. This equation began its derivation in *Murnaghan, 1937* relating the finite eulerian strain (f) of compressing from atomic position  $a_p \rightarrow x_p$  of an isotropic solid with density ( $\rho$ ) to the applied stress ( $\epsilon$ ) on the solid, resulting in a partial differential equation relating the two through the Helmholtz free energy, H.

**Equation 2**  $f_{rs} = \frac{1}{2} \left( \delta_{rs} - \frac{\partial a(p)}{\partial x(r)} \frac{\partial a(p)}{\partial x(s)} \right)$

r, p, s = 1, 2, 3 and denote the strain components

**Equation 3**  $\varepsilon_{rs} = \rho \left( \frac{\partial H}{\partial f(r,s)} - 2f(r,p) \frac{\partial H}{\partial f(p,s)} \right)$

**Equation 4**  $H = E - TS$      $E =$  internal energy     $T =$  temperature     $S =$  entropy

This PDE equation was simplified for the highly symmetric case of a cubic solid and approximately evaluated by means of a Taylor expansion in the strain through the work of Francis Birch (*Birch 1947*). From here, the relation is further simplified by substitution of the commonly measured Bulk modulus. The derivation can be carried out to an infinite number of terms in the bulk modulus and strain but, the most commonly used is the third-order approximation which carries out to the first pressure derivative of the bulk modulus  $B_0'$  shown in:

**Equation 5**  $P(V) = \frac{3}{2} B_0 \left[ \left( \frac{V_0}{V} \right)^{\frac{7}{3}} - \left( \frac{V_0}{V} \right)^{\frac{5}{3}} \right] \left\{ 1 + \frac{3}{4} (B_0' - 4) \left[ \left( \frac{V_0}{V} \right)^{\frac{2}{3}} - 1 \right] \right\}$

If being evaluated for a material of ideal compression conditions (typically a cubic metal)  $B_0'$  can be held at a constant value of 4 which collapses the function into the second order Birch-Murnaghan EoS.

Nearly half a century later after much more empirical data had been established, a more 'universal' function was derived by the work of James H. Rose for metals at zero temperature and subsequently Pascal Vinet to include temperature effects in what was labeled the "Universal Equation of State of Solids" (*Rose et al. 1983*) (*Vinet et al. 1986*). This universal EoS or commonly called the Rose-Vinet or just Vinet EoS is theoretically derived, alongside empirical verification, based on the assumption that a universal relation emerges

at high compression relating the binding energy (E), Wigner-Seitz radius ( $r_{ws}$ ), bulk modulus and the assumption that at zero temperature:

**Equation 6**  $P(V) = -\frac{dE}{dV}$

Following these assumptions for a general atomic potential (covalent bonded metals) and comparisons to experimental data lead to the assumption to use a rapidly changing function (exponential) which is similarly simplified in terms of the Bulk modulus giving the Rose-Vinet EoS currently being used for isothermal compression data:

**Equation 7** 
$$P(V) = 3 B_0 \left[ \frac{\left(1 - \left(\frac{V}{V_0}\right)^{\frac{1}{3}}\right)}{\left(\frac{V}{V_0}\right)^{\frac{2}{3}}}\right] \left[ e^{\frac{3}{2}(B_0' - 1)\left(1 - \left(\frac{V}{V_0}\right)^{\frac{1}{3}}\right)} \right]$$

The unclear phase boundary between ice-VII and ice-X, as well as the possibility of the intermediate ice-VII' makes fitting a single EoS meaningless as each phase is described by a separate ground state. These issues become evident when reviewing the literature on the EoS of H<sub>2</sub>O which gives highly scattered values for the bulk modulus between different experiments and different fitting procedures. The first EoS experiment of H<sub>2</sub>O is *Hemley et al. 1987* in which energy dispersive XRD was used to 128 GPa and the volume was obtained from one or two diffraction peaks; resulting in values of  $B_0 = 23.7(0.9)$  GPa,  $B_0' = 4.15(0.07)$ . A decade later, a study by *Wolanin et al. 1997* made measurements to 106 GPa and reported a bulk modulus nearly half that using both BM and Vinet EoS:  $B_0 = 14.9 (0.)$  GPa,  $B_0' = 5.4(0.1)$ . This study also commented on the possibility of a second or higher

order phase transition occurring which may be causing the discrepancy between the two works. *Loubeyre et al. 1999* fit their compression data, which went up to 170 GPa, using the Vinet EoS and obtained a value of  $B_0 = 4.26$  GPa,  $B_0' = 7.75$ . Discrepancies of this magnitude between data acquired under relatively similar conditions reveals that there is a fundamental issue in these studies.

**X-ray Diffraction:**

X-ray diffraction (XRD) is a method of probing the structure of a material by scattering of monochromatic (single wavelength,  $\lambda$ ) or polychromatic (continuous spectrum of wavelengths) X-ray beams from the electron distribution of a material. Initially, the x-rays propagate into the material with wave vector  $\mathbf{k}_{in}$  where:

**Equation 8** 
$$\mathbf{k} = \frac{2\pi}{\lambda}(\mathbf{x}, \mathbf{y}, \mathbf{z})$$

and are elastically scattered from the electron density in the material to some new direction  $\mathbf{k}_{out}$ . Because of the periodic 'd' spacing of planes in a lattice the scattering process results in a constructive interference pattern for x-rays with wavelength,  $\lambda$ , scattered off of periodic lattice distances, d, to some angle,  $\theta$ , determined by the Bragg condition:

**Equation 9** 
$$n\lambda = 2d\sin(\theta) \quad n = 1, 2, 3\dots$$

However most crystals are three dimensional with lattice dimensions: a, b and c. This three dimensional symmetry gives rise to many periodic two dimensional planes within the unit cell which are defined by the occupied sites in the reciprocal space unit cell known as the Miller indices (h, k, l). Only planes of the lattice that are parallel to the scattering vector ( $\mathbf{k}_{out} - \mathbf{k}_{in}$ ) are sampled. Thus, the possible planes (h, k, l) that are sampled are dependent

on the orientation between the crystal grain and the incoming and outgoing X-rays which is summarized in the Laue condition:

$$\text{Equation 10 } (\mathbf{a}, \mathbf{b}, \mathbf{c}) \cdot (\mathbf{k}_{\text{out}} - \mathbf{k}_{\text{in}}) = 2\pi(h, k, l)$$

The d-spacing measured from the observed angle of the diffraction fringe is indexed to its corresponding lattice plane and the lattice dimensions that give rise to that plane are related in the most general form by:

$$\text{Equation 11 } \frac{1}{d^2} = \frac{h^2}{a^2} + \frac{k^2}{b^2} + \frac{l^2}{c^2}$$

For an individual crystal in one specific orientation with respect to the incoming X-rays a single diffraction peak for a single plane is obtained. In order to acquire diffraction peaks from all lattice planes to get a full description of the sample one must rotate the orientation of the single crystal. Use of a single crystal is ideal for understanding the fundamental structural traits of a material by limiting distortions at grain-grain boundary interactions but, is not suitable for high pressure experiments in diamond anvil cells because the angular range is limited to a maximum of about 35°. To avoid the cumbersome work of performing multiple DAC loadings each containing a single crystal in a different orientation, it is common to use powder-XRD. This involves using a very fine powdered sample rather than a single crystal. The benefit of this method is that the powder is made up of a large



number of grains with random orientation and, if the grain size is much smaller than the X-ray beam that is being used, all possible lattice planes can be sampled in a single orientation of the DAC. Rather than the single crystal peak, powder diffraction results in the formation of concentric diffraction rings for each single d-spacing which are called Debye-Scherrer rings. Formation of a well powdered H<sub>2</sub>O ice-VII sample has proven difficult because it is practical to load the sample in the liquid but, the pressure induced crystallization of ice-VII results in grain sizes larger than the ~5 μm x-ray beam diameter which produce strained single crystal or poor multigrain patterns (Fig. 2).

**Methods:**

Bond states in soft molecular compounds, like ice, are strongly affected by non-hydrostatic stress at high pressure conditions. While non-hydrostatic conditions can normally be eliminated by the use of a fluid pressure transmitting media (*Klotz et al. 2009*); this cannot be reliably done in studies of pure H<sub>2</sub>O because of its tendency to incorporate noble gases or other materials into the ice structure in the form of clathrates or other hydrates. The resulting distortions are further exacerbated by the heterogeneous nucleation of ice-VII within ice-VI, yielding large crystalline domains that cause significant anisotropic effects at grain boundaries (Fig. 2).

To minimize these effects, we directly heat ice samples at pressure with a CO<sub>2</sub> laser until we observe bulk melting, and let the sample cool in ambient air back to room temperature. This technique is analogous to a common heat treatment method in metallurgy known as normalizing, in which steel is heated to a temperature above the phase transition to austenite and left to air cool resulting in normalizing the grain structure to a much finer size. Other than the maximum temperature, normalizing differs from other heat treatments in the cool-down rate which lies in a middle region between fast quenching by means of a water bath and the prolonged cooling in annealing techniques which are typically over hour time scales.

We observe several benefits of this direct heating technique: anisotropic strains within both the sample and the Au pressure marker are annealed (minimizing deviatoric stress for more accurate volume determination), recrystallization of the ice produces a normalized powdered sample with nanoscopic domains and, we eliminate the need to introduce an opaque coupler used in indirect heating with 1 $\mu$ m lasers. This elimination of

an opaque coupler is imperative to heating the sample uniformly opposed to the significant thermal gradient going from the opaque coupler to diamond and reducing the risk of unwanted chemistry between the heated water sample and typically metallic coupler. The reduced domain size yields well-resolved Debye-Scherrer fringes over an extensive d-range, making our data suitable for Rietveld powder x-ray diffraction analysis (Fig. 2). The powdered nature of the sample also reduces its susceptibility to further strain as compression continues, and increases the statistical weight of the collected data allowing for proper analysis of any Bragg peak splitting due to a lowering of crystallographic symmetry. Data that have not been recrystallized from the melt display significantly fewer diffraction features and typically exhibit poor multi-grain spots or highly textured rings with significant peak broadening from deviatoric stress (Fig. 2). By laser annealing the sample the full width half max can be reduced by a factor of 2. For example, the full-width-half-max of the 1 1 0 peak (first peak) in Fig. 2 improves from  $0.24^\circ$  in the non-heated pattern to  $0.088^\circ$  in the heated pattern.

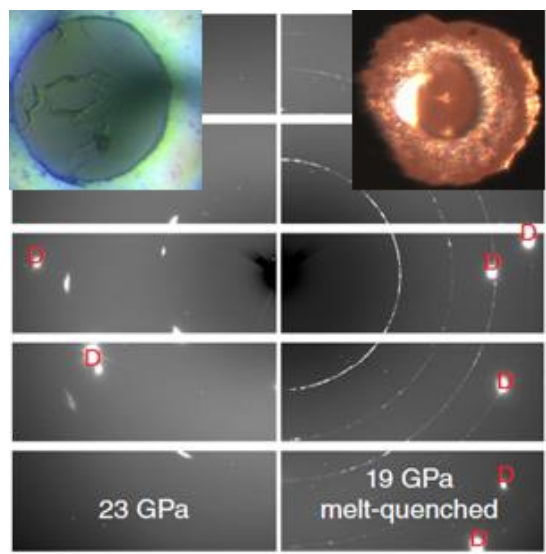


**Figure 2: Comparison of XRD 2-D images on *Pilatus* detector for ice-VII. Left: compression of large ice grains that have not been recrystallized from melt showing significant texturing and peak broadening and microscope image showing large crystallite domains. Right: Improved powder diffraction which has been annealed and recrystallized from melt and image of the melt bubble formed when laser heating with nanoscopic domains recrystallizing around it. Red 'Ds' denote single crystal reflections from the diamond anvils**

Pressure-volume measurements were performed using a DAC of custom design manufactured by Paul Ellison of the UNLV Physics machine shop, driven by a gas membrane. Diamond culet sizes were in the range from 100-300  $\mu\text{m}$ .  $\text{H}_2\text{O}$  (electrophoresis and spectroscopic grade; Sigma-Aldrich) was loaded in the liquid phase with an approximately 10  $\mu\text{m}$  piece of polycrystalline Au, to serve as a pressure marker, into sample chambers formed by laser micromachining of the pre-indented Re gasket. Evidence of reactions between the laser heated  $\text{H}_2\text{O}$  sample and the Re gasket had been observed in early experiments by means of gasket failure and characterization of a rhenium-oxide on the surface of the recovered gasket. To avoid this issue all gaskets in this experiment were made with a Pt lining, isolating the sample from the Re (Fig. 3).

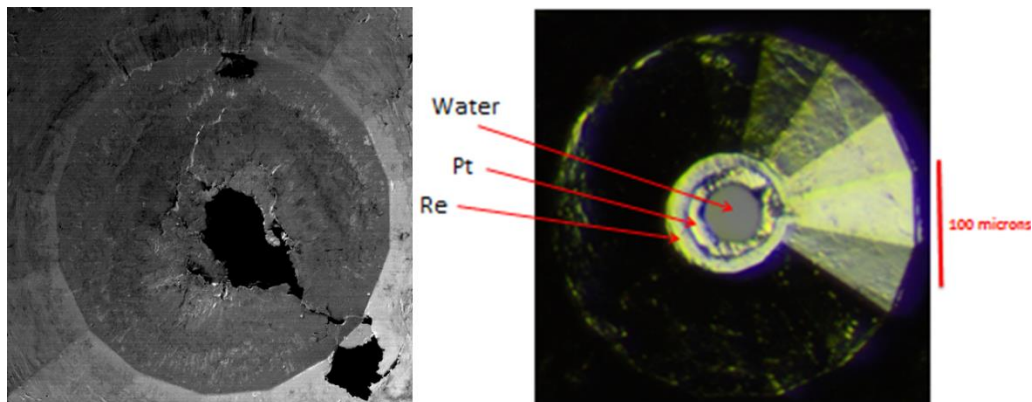


**Figure 3: Platinum lined gasket. Left: SEM image of recovered gasket after severe failure during heating experiment. Right: modified gasket with Pt lining to prevent reaction of heated sample with Re.**

X-ray diffraction was conducted at the HPCAT diffraction beamline (Sector 16, Advanced Photon Source, Argonne National Laboratory, IL, USA) using a monochromatic beam with wavelength  $\lambda = 0.406626 \text{ \AA}$ . Two-dimensional XRD patterns, like those in Fig. 2, are integrated into conventional one-dimensional spectra with the DIOPTAS software package, and Rietveld refinements performed using GSAS. Volumes are indexed using a Le Bail extraction assuming a cubic ( $Pn-3m$ ) cell. Pressure is determined by indexing the Au pressure marker, and comparing the volume to the known equation of state (*Dewaele et al. 2004*). Uncertainties in pressure are given from the average deviations between the volume given by the full-spectrum fit to the Au, and those found from indexing the (1 1 1) and (2 0 0) peaks individually, in order to give more weight to points that experience less deviatoric stress.

The cell was loaded and closed so that the water was still in its liquid phase, as confirmed by the broad liquid diffraction ‘halo’ in Fig. 4. To prepare a single phase of powdered water ice under high pressure, we utilize its high absorbance in the mid-infrared

and the fine pressure control provided by a gas-membrane compression system. At the first observation *via* x-ray diffraction of phase coexistence between ice-VI and ice-VII, 10.6  $\mu\text{m}$  radiation from a Synrad *Evolution*125 CO<sub>2</sub> laser is focused to a minimum spot size  $\sim 50 \mu\text{m}$  through the diamond anvil and directly onto the compressed sample, using an instrument built in-place at the HPCAT diffraction beamline (Sector 16, Advanced Photon Source, Argonne National Laboratory, IL, USA), or on a system housed at UNLV. Visible imaging confirms the formation of the melt within the solidified sample by lensing of transmitted light through a melted volume surrounded by dynamically recrystallizing powdered ice of a normalized grain size. The focused beam is translated throughout the sample chamber, in this way; both the powder and the Au pressure marker are thoroughly annealed. After cooling to room temperature a single phase of pure ice-VII is observed. This enables us to begin measurements on the phase at the very beginning of its field of thermodynamic stability giving accurate determination of the starting volume,  $V_p$ , of ice-VII at the transition pressure. Good powder quality is obtained *via* this method up to 88 GPa. At higher pressures ( $>50$  GPa), a melt is not always achieved due to either: lower absorption of the mid-IR radiation or the high melting point of ice at these pressures. In these cases, CO<sub>2</sub> laser heating is employed to anneal the powdered ice sample that was formed at lower pressures – observable in the reduction of Bragg peak widths.

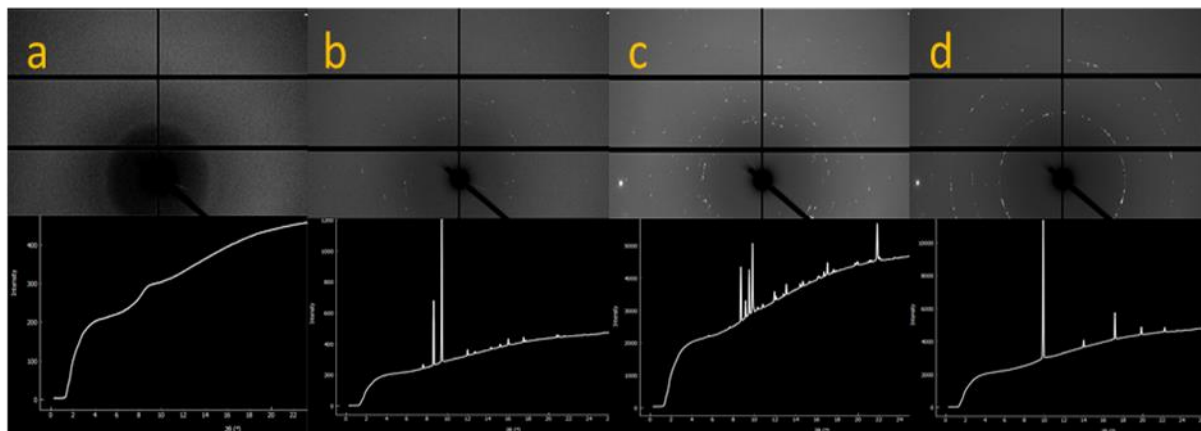


**Figure 4: Preparation of powdered ice-VII. a) Diffraction 'halo' from liquid structure factor of H<sub>2</sub>O before solidification. b) Solidification of ice-VI. c) Emergence of ice-VII within ice-VI before heating. d) Pure ice-VII sample achieved after heating the mixed phase sample into the melt then recrystallizing and cooling back to room temperature.**

## Results:

The resulting pressure-volume relation is shown in Fig. 5. From here, a least squares fitting technique is used to fit the Birch-Murnaghan (BM) and Rose-Vinet (RV) EoS functions to our data shown in (Fig 5.). Both result in similar fitted parameters ( $B_0 = 26.13 \pm 0.40$  GPa,  $B_0' = 5.51 \pm 0.07$ ,  $V_0 = 38.56 \pm 0.09 \text{ \AA}^3$ ), which is approximately 30% less compressible than the most recent measurements made by *Bezacier et al. 2014*. However, the fitted curve does not truly represent the P-V data over the full pressure range but rather, intercepts through the center of the data. To further investigate if the fitted curve represents the data a linearized EoS method outlined by *Jeanloz 1981* and *Angel 2000* was used to test the validity of the parameters acquired from the single phase EoS fit. This technique involves a transformation of our P-V data to a normalized pressure ( $F_V$ ) vs. strain ( $f$ ) plot.

**Equation 12**      
$$F_V = \ln\left(\frac{P*f}{3(1-f)}\right)$$

The criterion for the fit parameters to be a good description of the data in question is defined by the P-V data being transformed into a straight line, while a plot with significant curvature demonstrates a poor fit. A straight line with a slope of 0 indicates that the BM equation can be shortened to a 2<sup>nd</sup> order ( $B_0' = 4$ ), a positive slope results in a pressure derivative greater than 4 and a negative slope less than 4. Similarly the intercept on the normalized pressure axis defines the bulk modulus. When this transformation is applied to the data presented here using a single phase fit the resulting curve has an abnormal curvature (Fig. 5) signifying a failure of the fitting parameters to model the data correctly.



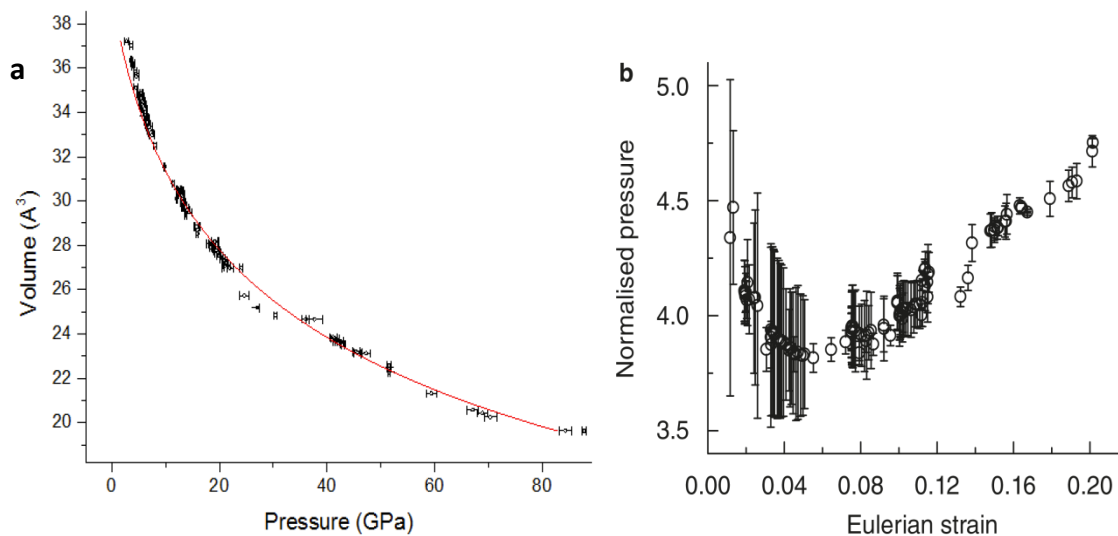


**Figure 5: Demonstration of failure to fit data to a single phase. a) Poor modeling of fitting a single Rose-Vinet EoS to the full pressure range. b) Abnormal curvature obtained when transforming data to the linearized Rose-Vinet EoS further signifying a failure of the single phase model.**

With the linearized form validating the poor fit to the full pressure range of our data a more critical look is needed. The wealth of previous studies point to the possibility of two phase transitions occurring within the pressure range spanned in this experiment. The first is a disordered phase ice-VII' that had been observed near 12-14 GPa. This is supported by neutron diffraction (*Guthrie & Boehler, 2013*) showing evidence for protons occupying interstitial sites and in XRD (*Somayazulu et al. 2008*) which attempts to fit a tetragonal structure. When looking at the data acquired in this experiment, there are clear deviations in peak positions with respect to the cubic,  $Pn-3m$ , model being used particularly, possible splitting of the 200/002 peak as observed by the increased skewness

of the peak profile. This deviation from the cubic model begins to appear near 5 GPa which is preceded by a minute volume collapse of 2.12(0.01)% (Fig. 6). Acknowledging the previous work claiming structural peculiarities and our own observation, we re-investigate our XRD data with a Rietveld fit which relies heavily on the relative intensity of each peak in the diffraction spectrum and its relation to the position and charge of each atom in the unit cell. We compare Rietveld refinements using the cubic  $Pn-3m$  structure to fits using a lower symmetry sub-group of the cubic model to see if it improves our fit. Of these options, the tetragonal subgroup,  $P4_2/nnm$ , increases the goodness of fit of our Rietveld refinement (Rwp=2.36% for cubic  $a = 3.2275 \pm 0.0002 \text{ \AA}$  and Rwp=1.81% for tetragonal  $a = 3.2279 \pm 0.0002 \text{ \AA}$  and  $c = 3.2372 \pm 0.0003$ ).

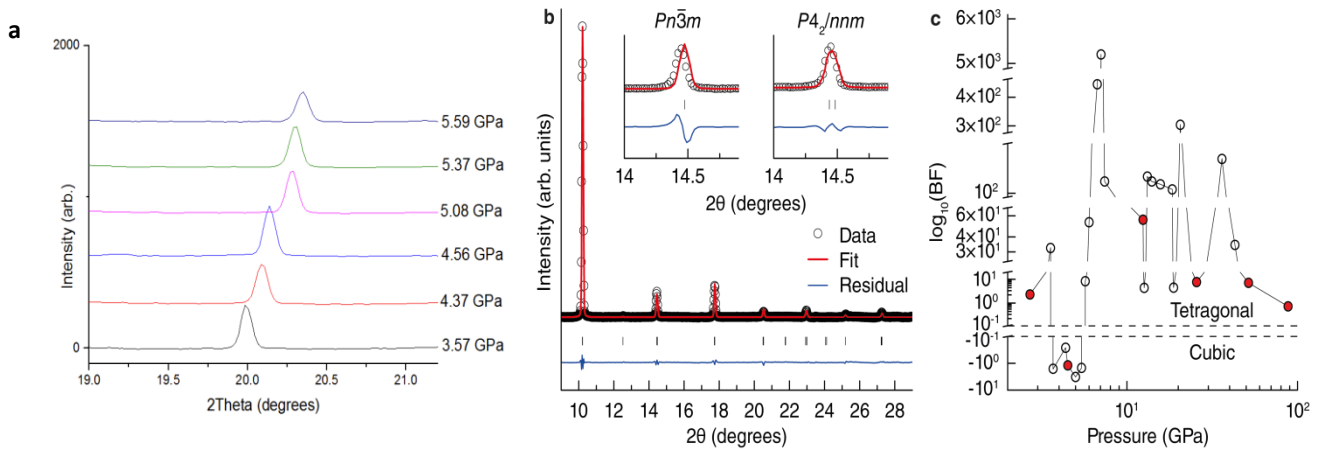


**Figure 6: Evidence for transition to tetragonal ice-VII<sub>t</sub>.** a) Discontinuity in volume from 4.56GPa to 5.08 GPa corresponding to a 2.12(0.01)% volume collapse. b) Improved Rietveld refinement when using tetragonal  $P4_2/nnm$  model as compared to bcc  $Pn-3m$  model and close up of the 200/002 peak which before and after fitting with tetragonal model. c) Bayesian model comparison showing relative probability of a tetragonal model vs. cubic over the pressure range of this experiment.

Our observation of a volume discontinuity and symmetry lowering has led us to accept the viability for the case of a transition to a tetragonal ice, which we label ice-VII<sub>t</sub>. In

this light, we reached out to collaborate with Jason Steffen and John Boisvert who are experts in model comparison algorithms. For this, Pseudo-Voigt fits are performed to each individual peak in the spectrum of each data point. Then the centroid and standard deviation of each peak is put into the algorithm. From here a Bayesian probability calculation is performed for the full spectra using the peak positions and widths as well as the lattice parameter obtained from fitting the full diffraction image together (*Boisvert et al. 2018*). This compares the likelihood of  $a=b=c$  (cubic model) versus that of  $a=b\neq c$  (tetragonal model). The resulting probabilities are plotted as a function of pressure (Fig. 6). This plots points that favor a cubic model below unity (one) and those that favor a tetragonal model above unity. A clear trend is observed as above 5 GPa the tetragonal model shoots up becoming increasingly viable by many orders of magnitude. Then at pressures above 30 GPa the cubic model begins to become increasingly viable again. Observing this trend gives us confidence in claiming the transition to a tetragonal symmetry and also led our decision in investigating the possibility of a transition to a higher symmetry structure above 30 GPa.

Upon further inspection it is evident that near 30 GPa the P-V curve becomes abruptly less compressible. It is likely this was the cause of the more incompressible EoS fit parameters when using a single phase model. This is below the pressure that previous experiments have claimed the transition to symmetric ice-X but, the stiffer ionic bond in this phase could account for this incompressibility. Claims of an ice-VII to X transition were first made via XRD at 40 GPa based on observation of this decrease in compressibility as well as analysis of the 111 diffraction peak, which is purely an artifact from the proton position in the ice crystal, compared to the 222 peak which is dominated by the oxygen

(Loubeyre *et al.* 1999). This analysis showed evidence of flattening of the relative intensity between the two peaks, which was interpreted as the transition to the proton occupying the symmetric point between adjacent oxygens characteristic of a transition to the ionically bonded symmetric ice-X. Ionic bonds are characteristically stronger by 2 to 3 orders of magnitude (600 to 4000 kJ/mol) than that of an H-bond (6 to 23 kJ/mol). Following the derivation of compressibility in *Born & Huang, 1954*, in which the dipole-dipole interaction of neighboring atoms results in an equation of motion analogous to that of a coupled oscillator, this large increase in bond energy is a transition to an extremely stiff spring constant connecting the atoms in the crystal. This ‘bond stiffening’ is inversely related to the compressibility, resulting in ionic ice-X being much less compressible (larger bulk modulus) than the loose H-bond network in all other ices. Our combined observation of an abrupt decrease in compressibility and the increased symmetry at this pressure range combined with direction from literature, guides our decision in claiming this as a transition to ionic bonded, ice-X.

EoS fits were performed to these three regions separately using traditional least-squares fitting assuming transition pressures at 5 and 30 GPa by me. Simultaneously, John Boisvert also fit the regions using a more sophisticated, Markov-Chain Monte Carlo (MCMC) algorithm where the transition pressure was also left as fitting parameter to quantify a value rather than using experimental intuition. This resulted in improved agreement between the EoS models (Fig. 7) and our data as well as agreement between the obtained fitting parameters between the least-squares fitting and MCMC fitting. The latter resulted in transition pressure to ice-VII<sub>t</sub> at  $4.78 \pm 0.76$  GPa and to ice-X at  $30.91 \pm 2.90$  GPa. Subsequently the linearized form is used again to test if the fitted parameters correctly

model the three regions (Fig. 7). The resulting transformation shows clear linear trends in each of the three regions which further support the use of the three phase model over this pressure range.

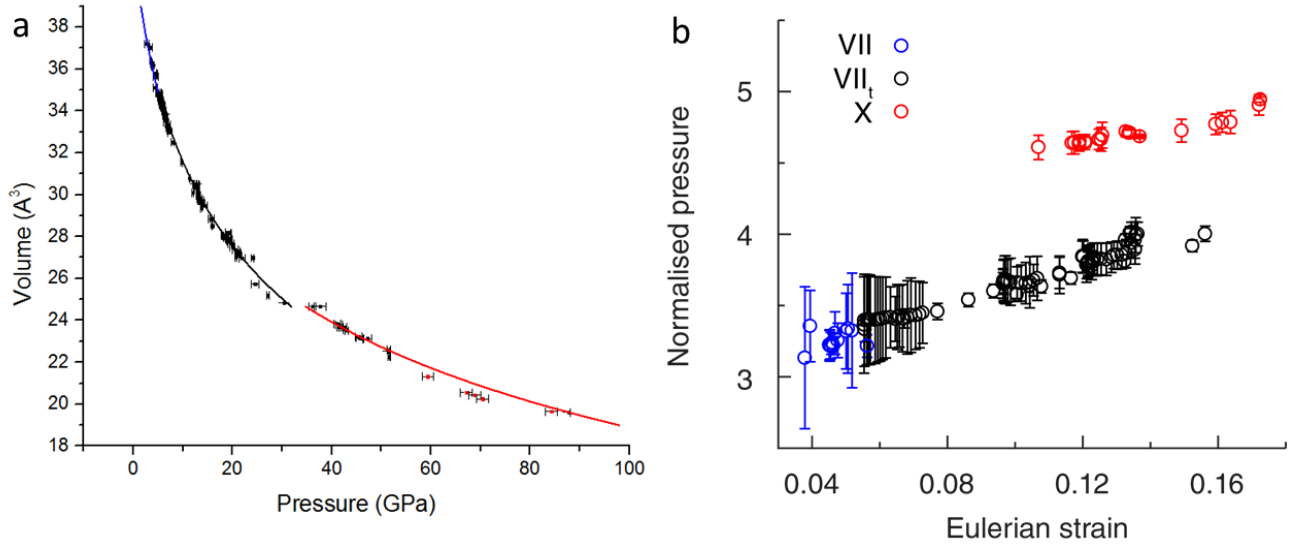


**Figure 7: Successful fit using 3 phase model. Cubic ice-VII from  $2.71 \pm 0.43$  to  $4.78 \pm 0.76$  GPa, tetragonal ice-VII<sub>t</sub> from  $4.78 \pm 0.76$  GPa to  $30.9 \pm 2.9$  GPa, and ionic ice-X thereafter. a) Three phase EoS fit to data, red points represent data from decompression which exhibit hysteresis. (blue: cubic ice-VII ( $B_0 = 18.47 \pm 4.00$  GPa,  $B_0' = 2.51 \pm 1.51$ ,  $V_0 = 42.50 \pm 0.88$  Å<sup>3</sup>), black: non-cubic ice-VII<sub>t</sub> ( $B_0 = 20.76 \pm 2.46$  GPa,  $B_0' = 4.49 \pm 0.35$ ,  $V_0 = 41.11 \pm 0.53$  Å<sup>3</sup>), and red: ice-X ( $B_0 = 50.52 \pm 4.16$  GPa,  $B_0' = 4.50 \pm 0.15$ ,  $V_0 = 33.82 \pm 0.43$  Å<sup>3</sup>)) b) Linearized Rose-Vinet EoS and clear linear trend obtained from the using the fitted parameters in the transformation.**

**Conclusion:**

The results of the multi-phase EoS fit show that room temperature H<sub>2</sub>O takes the form of cubic ice-VII from  $2.71 \pm 0.43$  to  $4.78 \pm 0.76$  GPa, followed by tetragonal ice-VII<sub>t</sub> to  $30.9 \pm 2.9$  GPa, then cubic ice-X thereafter. The low transition pressure into non-cubic ice-VII<sub>t</sub> implies that cubic ice-VII is stable for only a small window of phase space – contrary to existing assumptions (*Holzappel, 1972*). A 2.5-fold increase in bulk modulus at  $30.9 \pm 2.9$  GPa by definition signifies an abrupt increase in bond strength, which we interpret as the transition from H-bonded ice-VII<sub>t</sub> to ionic-bonded ice-X (*Born et al. 1954*).

Interestingly, there is an abrupt steepening of the melt curve above 40 GPa which must result from a change in thermodynamic properties either within the fluid phase above, or the solid phases below (Fig. 8)(*Schwager & Boehler 2008, Goncharov et al. 2009*). The transition to a stronger ionic bond in ice-X, like the one presented here, can explain this inflection near 44 GPa, (*Schwager & Boehler 2008, Goncharov et al. 2009*) resulting in a steep, positive Clapeyron slope at the phase boundary as shown in Fig. 8. This interpretation is in compliance with the observation of a molecular-to-ionic transition in warm dense H<sub>2</sub>O above 40 GPa (*Schwager & Boehler 2008, Goncharov et al. 2009, Goncharov et al. 2005*). Also, commonly related to this region of interest is the occurrence of superionic ice, an ionized solid state in-which the hydrogen have become fully delocalized and able to freely diffuse through the lattice, as an intermediate phase between ice-X and melt at around 50 GPa (*Sugimura et al. 2012, Millot et al. 2018*). Hence, the transition from H-bonded to ionic H<sub>2</sub>O (solid black lines in Fig. 8) is not strongly temperature-dependent, as expected for a pressure-driven change in chemical bonding.

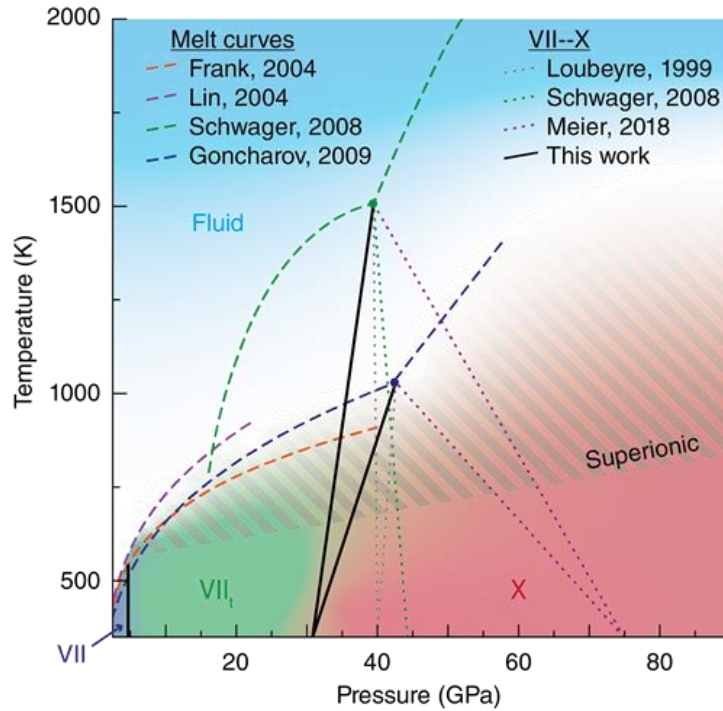


**Figure 8: High-pressure high-temperature phase diagram of H<sub>2</sub>O.** Dark blue, green and red shaded regions denote ice-VII, VII<sub>t</sub> and X, respectively, and projected phase boundaries separating high-pressure ice phases from our work are shown as solid black lines. Ice-X phase boundaries connect our measured transition at  $30.91 \pm 2.90$  GPa and 300 K to the inflexion point in the melt curve observed by Schwager *et al.* 2008 and Goncharov *et al.* 2009, which have been associated with the transition from molecular to ionic fluid. The same procedure has been used to project phase boundaries from Loubeyre *et al.* 1999 and Meier *et al.* 2018. In doing so, we deduce a steep, positive Clapeyron slope defining the transition from hydrogen bonding to ionic bonding in dense H<sub>2</sub>O, consistent with a pressure-driven change in bonding nature. Dashed lines show measured melting curves. Superionic boundary from Sugimura *et al.* 2012 is highlighted.

## **Bibliography:**

- Angel, R. J. (2000). Equations of state. *Reviews in mineralogy and geochemistry*, 41(1), 35-59.
- Bezacier, L., Journaux, B., Perrillat, J. P., Cardon, H., Hanfland, M., & Daniel, I. (2014). Equations of state of ice VI and ice VII at high pressure and high temperature. *The Journal of chemical physics*, 141(10), 104505.
- Birch, F. (1947). Finite elastic strain of cubic crystals. *Physical review*, 71(11), 809.
- Boisvert, J. H., Nelson, B. E., & Steffen, J. H. (2018). Systematic mischaracterization of exoplanetary system dynamical histories from a model degeneracy near mean-motion resonance. *Monthly Notices of the Royal Astronomical Society*, 480(2), 2846-2852.
- Born, M., & Huang, K. (1954). *Dynamical theory of crystal lattices*. Clarendon press.
- Bridgman, P. W. (1912, January). Water, in the liquid and five solid forms, under pressure. In *Proceedings of the American Academy of Arts and Sciences* (Vol. 47, No. 13, pp. 441-558). American Academy of Arts & Sciences.
- Bridgman, P. W. (1937). The phase diagram of water to 45,000 kg/cm<sup>2</sup>. *The Journal of Chemical Physics*, 5(12), 964-966.
- Dewaele, A., Loubeyre, P., & Mezouar, M. (2004). Equations of state of six metals above 94 GPa. *Physical Review B*, 70(9), 094112.
- Dunaeva, A. N., Antsyshkin, D. V., & Kuskov, O. L. (2010). Phase diagram of H<sub>2</sub>O: Thermodynamic functions of the phase transitions of high-pressure ices. *Solar System Research*, 44(3), 202-222.
- Frank, M. R., Fei, Y., & Hu, J. (2004). Constraining the equation of state of fluid H<sub>2</sub>O to 80 GPa using the melting curve, bulk modulus, and thermal expansivity of Ice VII. *Geochimica et cosmochimica acta*, 68(13), 2781-2790.
- Goncharov, A. F., Goldman, N., Fried, L. E., Crowhurst, J. C., Kuo, I. F. W., Mundy, C. J., & Zaug, J. M. (2005). Dynamic ionization of water under extreme conditions. *Physical review letters*, 94(12), 125508.
- Goncharov, A. F., Sanloup, C., Goldman, N., Crowhurst, J. C., Bastea, S., Howard, W. M., ... & Meng, Y. (2009). Dissociative melting of ice VII at high pressure. *The Journal of chemical physics*, 130(12), 124514.
- Goncharov, A. F., Struzhkin, V. V., Mao, H. K., & Hemley, R. J. (1999). Raman spectroscopy of dense H<sub>2</sub>O and the transition to symmetric hydrogen bonds. *Physical Review Letters*, 83(10), 1998.
- Goncharov, A. F., Struzhkin, V. V., Somayazulu, M. S., Hemley, R. J., & Mao, H. K. (1996). Compression of ice to 210 gigapascals: Infrared evidence for a symmetric hydrogen-bonded phase. *Science*, 273(5272), 218-220.



- Guthrie, M., Boehler, R., Tulk, C. A., Molaison, J. J., dos Santos, A. M., Li, K., & Hemley, R. J. (2013). Neutron diffraction observations of interstitial protons in dense ice. *Proceedings of the National Academy of Sciences*, *110*(26), 10552-10556.
- Hemley, R. J., Jephcoat, A. P., Mao, H. K., Zha, C. S., Finger, L. W., & Cox, D. E. (1987). Static compression of H<sub>2</sub>O-ice to 128 GPa (1.28 Mbar). *Nature*, *330*(6150), 737.
- Holzappel, W. B. (1972). On the symmetry of the hydrogen bonds in ice VII. *The Journal of Chemical Physics*, *56*(2), 712-715.
- Holzappel, W. B., Seiler, B., & Nicol, M. (1984). Effect of pressure on infrared-spectra of ice VII. *Journal of Geophysical Research: Solid Earth*, *89*(S02).
- Jeanloz, R. (1981). Finite-strain equation of state for high-pressure phases. *Geophysical Research Letters*, *8*(12), 1219-1222.
- Klotz, S., Chervin, J. C., Munsch, P., & Le Marchand, G. (2009). Hydrostatic limits of 11 pressure transmitting media. *Journal of Physics D: Applied Physics*, *42*(7), 075413.
- Lin, J. F., Militzer, B., Struzhkin, V. V., Gregoryanz, E., Hemley, R. J., & Mao, H. K. (2004). High pressure-temperature Raman measurements of H<sub>2</sub>O melting to 22 GPa and 900 K. *The Journal of chemical physics*, *121*(17), 8423-8427.
- Loubeyre, P., LeToullec, R., Wolanin, E., Hanfland, M., & Hausermann, D. (1999). Modulated phases and proton centring in ice observed by X-ray diffraction up to 170 GPa. *Nature*, *397*(6719), 503.
- Meier, T., Petitgirard, S., Khandarkhaeva, S., & Dubrovinsky, L. (2018). Observation of nuclear quantum effects and hydrogen bond symmetrisation in high pressure ice. *Nature communications*, *9*(1), 2766.
- Millot, M., Hamel, S., Rygg, J. R., Celliers, P. M., Collins, G. W., Coppari, F., ... & Eggert, J. H. (2018). Experimental evidence for superionic water ice using shock compression. *Nature Physics*, *14*(3), 297.
- Murnaghan, F. D. (1937). Finite deformations of an elastic solid. *American Journal of Mathematics*, *59*(2), 235-260.
- Rose, J. H., Smith, J. R., & Ferrante, J. (1983). Universal features of bonding in metals. *Physical review B*, *28*(4), 1835.
- Schwager, B., & Boehler, R. (2008). H<sub>2</sub>O: another ice phase and its melting curve. *High Pressure Research*, *28*(3), 431-433.
- Somayazulu, M., Shu, J., Zha, C. S., Goncharov, A. F., Tschauer, O., Mao, H. K., & Hemley, R. J. (2008). In situ high-pressure x-ray diffraction study of H<sub>2</sub>O ice VII. *The Journal of chemical physics*, *128*(6), 064510.

Sugimura, E., Komabayashi, T., Ohta, K., Hirose, K., Ohishi, Y., & Dubrovinsky, L. S. (2012). Experimental evidence of superionic conduction in H<sub>2</sub>O ice. *The Journal of chemical physics*, 137(19), 194505.

Verne, J. (2003). *A Journey to the Center of the Earth*. Penguin.

Vinet, P. J. J. R., Ferrante, J., Smith, J. R., & Rose, J. H. (1986). A universal equation of state for solids. *Journal of Physics C: Solid State Physics*, 19(20), L467.

Wolanin, E., Pruzan, P., Chervin, J. C., Canny, B., Gauthier, M., Häusermann, D., & Hanfland, M. (1997). Equation of state of ice VII up to 106 GPa. *Physical Review B*, 56(10), 5781.

Zha, C. S., Tse, J. S., & Bassett, W. A. (2016). New Raman measurements for H<sub>2</sub>O ice VII in the range of 300 cm<sup>-1</sup> to 4000 cm<sup>-1</sup> at pressures up to 120 GPa. *The Journal of chemical physics*, 145(12), 124315.

## Curriculum Vitae:

# Zachary M. Grande

zachgrande@gmail.com

---

Department of Physics and Astronomy,

University of Nevada, Las Vegas

---

### Experience/Skillset:

- X-ray Diffraction and Crystallography:
  - Monochromatic
    - APS, Argonne NL: 84 Shifts (2016-2018)
  - White Laue
    - APS, Argonne NL: 36 Shifts (2017-2018)
- Spectroscopy:
  - Raman at room and high temperatures
- High Pressure Science:
  - Diamond Anvil Cell (50-300  $\mu\text{m}$  culets)
- Laser Heating:
  - CO<sub>2</sub> Laser Heating in diamond anvil cells
- Apparatus Design and Fabrication:
  - Machining Techniques for Various Metals and Synthetics
    - Milling, Lathing, Welding
  - Motorized Mounts for Controlling Optics
  - Electronic Flood Censors for Research Lab
- Programming
  - C++
  - Quantum Computing Course Spring 2019

---

### Research Interests:

Exotic states of ices at pressures and temperatures that replicate the interiors of icy moons, Earth, super earths and ice giants with an emphasis on water: at multi-Megabar pressures, pyrometry measurements, and conductive states.

---

## Outreach/ Teaching Experience

- Teaching Assistant Fall 2016-Spring 2019
    - Instruct Undergraduate Lab Courses
  - Invited Speaker March 2019
    - Undergraduate Society of Physics Students
  - Extreme Crystals Workshop Volunteer 2016, 2017
- 

## Conferences/ Presentations:

- Gordon Research Conference on High Pressure July 2018
    - Invited Talk and Poster Presentation
  - 26<sup>th</sup> AIRAPT (Beijing, China) August 2017
  - SSAP (NNSA Symposium) Poster Presentation April 2017
  - Gordon Research Conference on High Pressure July 2016
- 

## Education:

- Master's of Science in Physics
    - May 2019 University of Nevada, Las Vegas
    - Dr. Ashkan Salamat (Advisor)
      - High Pressure and Temperature Ice: structure determination
    - Dr. Oliver Tschauner (Graduate Committee member)
      - Laue Diffraction of Low-Z materials
    - 3.4 GPA
  - Bachelors of Science in Physics
    - December 2015 University of Nevada, Las Vegas
    - Paul Ellison (Head Machinist)
      - Research Apparatus Design and Fabrication
        - Mechanical Design and Drawing Techniques
        - Machining Techniques
    - Dr. Victor Kwong (Advisor)
      - Ultra-High Vacuum Technology
      - AMO Research
        - Electron Transfer Research
-